Punching-shear resistance of point-supported CLT panels

Houman Ganjali, PhD candidate, University of Northern British Columbia (UNBC), Prince George, Canada; ganjali@unbc.ca

Thomas Tannert, UNBC, Prince George, Canada; thomas.tannert@unbc.ca

Md Shahnewaz, Fast + Epp, Vancouver, Canada; mshahnewaz@fastepp.com

Carla Dickof, Fast + Epp, Vancouver, Canada; cdickof@fastepp.com

Marjan Popovski, FPInnovations, Vancouver, Canada; marjan.popovski@fpinnovations.ca

Keywords: Floor systems, experimental investigation, shear analogy

1 Introduction

1.1 Background

Cross-laminated timber (CLT) has gained popularity in recent years as a sustainable and cost-effective alternative to traditional construction materials, particularly for floor applications (Karacabeyli & Gagnon, 2019). This includes point-supported flat-slabs, where the panels are supported directly by columns, without the need for beams and their connections (Popovski et al., 2016). One of the key properties in these applications is the CLT punching shear resistance, which refers to its ability to resist concentrated loads or "punching" through the material. The factors influencing CLT punching shear resistance are either material-strength-related or support-condition-related and should be accounted for in design.

1.2 CLT punching shear resistance

CLT punching shear resistance, R_{pu}, is directly related to the rolling shear strength, f_s, and impacted by the confinement of lamellas from adjacent layers and the presence of concurrent compression forces. These effects are accounted for in design by the rolling shear resistance in punching shear adjustment factor, $K_{r,pu}$, (Mestek, 2011; Bogensperger & Jöbstl, 2015; Muster, 2020). Mestek & Dietsch (2013) proposed an adjustment factor of 1.2; in Annex D of prEN1995 (2023) a $K_{r,pu}$ of 1.6 is recommended; and Muster (2020) proposed $K_{r,pu}$ of 1.6 and 1.3 for centre and corner columns.

While the Canadian Standard for Engineering Design in Wood CSA O86 (2024) provides specified f_s strength values of 0.5-0.66 MPa, the characteristic 5^{th}% f_s values of CLT panels from major Canadian providers (adjusted for normal duration of load) were reported to range from 0.54 MPa to 1.08 MPa (Ganjali et al., 2023).

Adopting an appropriate shear stress distribution model to estimate the actual stresses close to point-supports is crucial. prEN1995 (2023) recommends checking the rolling shear stress at an effective perimeter of the loaded area defined at 35° to the centre line of the CLT thickness. However, this provision lacks a clear analytical basis and does not provide any adjustment factors for support-condition, i.e. the effect of column location and geometry, which are required for efficient CLT punching shear design.

The Shear Analogy (SA) method is capable of accounting for the effect of transverse layers on the shear stress profile in CLT. In this method, based on the parallel axis theorem for determining the moment of inertia of a body about a given axis, the CLT panel is separated into two virtual beams, A and B, linked with infinitely rigid web (see Figure 1). The bending stiffness of beam A, (B_A), is the sum of the flexural stiffness of the individual layers along their own neutral axes Eq. 1, while beam B (B_B) provides the "Steiner" contribution to the effective flexural stiffness Eq. 2 (Kreuzinger 1999; Karacabeyli & Gagnon, 2019). Mestek (2011) proposed a simplified approach to determine the internal forces of the ideal beams without using a statics program.

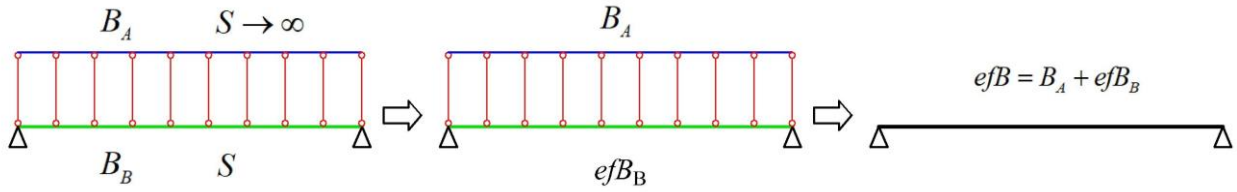

Figure 1. SA method representation of CLT panel as beam A and beam B.

$$B_A = \sum_{i=1}^{n} E_i \cdot I_i = \sum_{i=1}^{n} E_i \cdot b_i \cdot \frac{h_i^3}{12} \quad \text{Eq. 1}$$

$$B_B = \sum_{i=1}^{n} E_i \cdot A_i \cdot {z_i}^2 \quad \text{Eq. 2}$$

Where B_A is $(EI)_A$; b_i is the layer width; h_i is the layer thickness; B_B is $(EI)_B$, and z_i is the distance between the layer centre point and the panel neutral axis.

In the ideal rigid system in SA, the share of the internal shear forces (V_A and V_B) can thus be determined and assigned to beam A and B via the ratio of the bending stiffnesses:

$$V_A = V \cdot \frac{B_A}{efB} \quad \text{Eq. 3}$$

$$V_B = V \cdot \frac{efB_B}{efB} \quad \text{Eq. 4}$$

Where, V is the maximum external shear force on CLT from force analysis; and efB_B and efB are the effective bending stiffnesses of beam B and CLT (Mestek, 2011):

$$efB = B_A + efB_B \quad \text{Eq. 5}$$

$$efB_B = B_B \cdot \frac{1}{1 + \frac{B_B \cdot \pi^2}{S \cdot l^2}} \quad \text{Eq. 6}$$

where S is section modulus; and l is the length of the beam.

The rolling shear stress (τ_s) in each beam is calculated:

$$\tau_{s,A,i} = \frac{V_A \cdot E_i \cdot {h_i}^2}{8 \cdot B_A} \quad \text{Eq. 7}$$

$$\tau_{s,B,i} = \frac{V_B}{B_B} \cdot \sum_{1}^{i-1} E_i \cdot h_i \cdot z_i \quad \text{Eq. 8}$$

The rolling shear stress in the i^{th} layer of CLT panel, $\tau_{s,i}$, then is:

$$\tau_{s,i} = \tau_{s,B,i} + \tau_{s,A,i} \quad \text{Eq. 9}$$

While the SA method can be deemed adequate for estimating the bending stiffness, the transformed-section method (Dunham, 1944) can be more readily adopted to determine the stress distributions in composite materials. In this method, originally developed for reinforced concrete, the steel rebars are replaced by an equivalent area of concrete, $A_{trans.}$, (reference material), Eq. 10, through the ratio (n) of modulus of elasticity ($E_{ref.}$) of concrete to E_{steel}, Eq. 11; this approach results in an imaginary transformed beam made of the reference material that can be used thereafter to calculate the geometry properties of the section and determine shear and bending stresses (Eq. 12 and Eq. 13). This method is simpler than SA method and can be used for CLT, however its efficiency in terms of shear stress distribution in CLT needs to be investigated.

$$A_{trans} = \frac{A_{steel}}{n} \quad \text{Eq. 10}$$

$$n = \frac{E_{ref}}{E_{steel}} \quad \text{Eq. 11}$$

$$\tau = \frac{V \cdot Q}{I \cdot b} \quad \text{Eq. 12}$$

$$\sigma = \frac{M \cdot y}{I} \quad \text{Eq. 13}$$

Once a 2D finite element analysis (FEA) method is adopted to obtain internal shear forces and design shear stresses in the major and minor strength directions, CLT point supports should be modelled as surface supports. The elastic support stiffness ($C_{u,z}$) is a key modelling parameter (Muster, 2020) because it has a significant impact on the predicted forces and stresses on each column face (Slotboom et al., 2023). Muster (2020) proposed an equation for $C_{u,z}$ as a function of CLT thickness (Eq. 14). However, this model needs to be verified with experimental results.

$$C_{\mathrm{u,z,Muster}} = 10^{13} \cdot {t_{CLT}}^{-3.15} \ [\mathrm{kN/m^3}] \qquad \text{Eq. 14}$$

1.3 Objectives

While limited design provision for point-supported CLT floors is provided in prEN1995 (2023), the current North American standards (CSA O86, 2024; NDS, 2024) do not include such guidance. To close this gap, a research project is being conducted by Fast + Epp structural engineers in collaboration with UNBC, consisting of four phases. The focus of this contribution is on phase (iii) with the objective to: a) investigate the effect of various support-condition-related parameters on CLT punching shear and ii) propose a more detailed CLT punching shear design provision.

2 Materials and Methods

2.1 Experimental investigation

The punching-shear resistance of 164 CLT panels from four Canadian manufacturers was evaluated to study the impact of: i) column location (edge, centre, corner, and perimeter, Figure 2, ii) grade (E1, V2), species (Spruce-Pine-Fir (SPF), Douglas Fir, and Hemlock), and layup (5-ply 175 mm thick and 7-ply 245 mm thick); and iii) column geometry and size (square, rectangle, round), see Figure 3. The E1 series had 1950 Fb-1.7E SPF and No.3 SPF in longitudinal and transverse layers, respectively. The V2 series had No.1/2 SPF and No.3/Stud SPF in in longitudinal and transverse layers, respectively, produced in accordance with ANSI/APA PRG 320. Series S4, S5, and S6 panels were edge glued. The panels were sized 1.7 m × 1.8 m, 1.5 m × 1.8 m, and 1.5 m ×1.5 m.

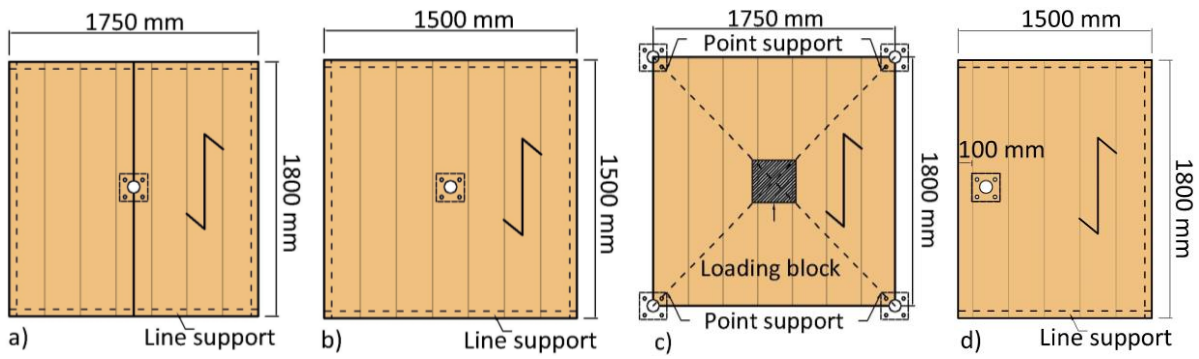

Figure 2. Punching shear test support locations: a) edge; b) centre; c) corner; and d) perimeter.

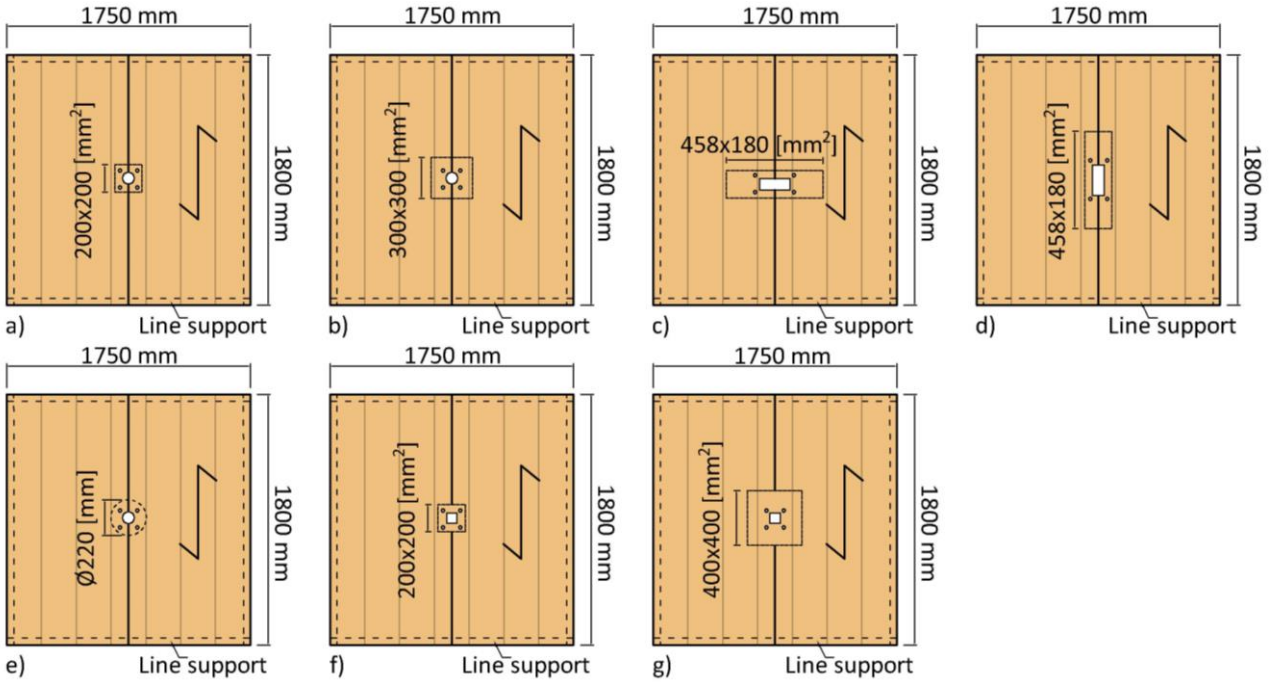

Figure 3. Different column geometries: a) square plate with stub (S1-S4, S6-S9, S15-S16); b) square plate with wood stub (S5); c) rectangular plate with wood stub (S10); d) rectangular plate with wood stub (S11); e) round column (S12); f) square plate and HSS (S13); and g) square plate and HSS (S14).

The edge and centre specimens were line-supported on four edges along the length, while the perimeter condition specimens were line-supported on three edges. The corner condition specimens were point-supported on four corners having the same bearing area, ensuring an equal possibility of failure for all corners. The test series overview is shown in Table 1. The tests were conducted according to ISO 6891 (1983) using a hydraulic actuator at a monotonic loading rate of 5 mm/min. The displacement of the tension side of the panels (underside for the edge, centre, and perimeter series and top for corner series) was recorded using string pots at various points throughout the tests. The typical test setup of each column condition is shown in Figure 4.

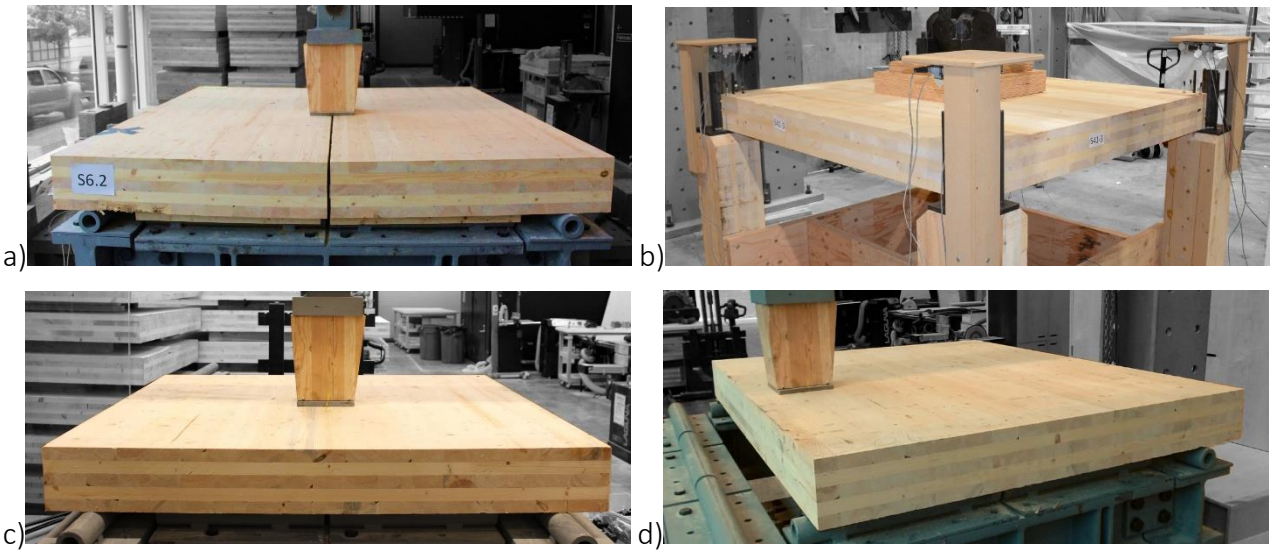

Figure 4. Typical a) edge; b) corner; c) centre; and d) perimeter setups.

Table 1. Overview of punching shear test series.

Series	Producer	Grade	CLT thick-ness [mm]	Species	Support dimen-sion [mm]	Column location
S1	D	V2	175	SPF	200 × 200	Edge
S2	D	E1	175	SPF	200 × 200	Edge
S3	A	E1	175	Spruce	200 × 200	Edge
S4	B	E1	175	SPF	200 × 200	Edge
S5	B	E1	175	SPF	300 × 300	Edge
S6	F	V2	175	SPF	200 × 200	Edge
S7	F	E1	175	SPF	200 × 200	Edge
S8	F	E1	175	D Fir	200 × 200	Edge
S9	F	E1	175	Hem	200 × 200	Edge
S10	F	E1	175	SPF	460 × 180	Edge
S11	F	E1	175	SPF	180 × 460	Edge
S12	F	E1	175	SPF	Ø 219	Edge
S13	F	E1	175	SPF	200 × 200	Edge
S14	F	E1	175	SPF	400 × 400	Edge
S15	F	E1	175	SPF	300 × 300	Edge
S16	F	E1	175	SPF	200 × 200	Edge
S17	F	E1	245	SPF	300 × 300	Edge
S23	F	E1	175	SPF	200 × 200	Edge
S24	F	E1	175	SPF	200 × 200	Centre
S25	F	E1	175	SPF	Ø 219	Centre
S26	F	E1	175	SPF	300 × 300	Centre
S27	F	E1	175	SPF	200 × 200	Centre
S28	F	E1	175	SPF	200 × 200	Centre
S29	F	E1	245	SPF	300 × 300	Centre
S30	F	E1	175	SPF	200 × 200	Perimeter
S41	F	E1	175	SPF	200 × 200	Corner
S42	F	E1	245	SPF	200 × 200	Corner

2.2 Analytical work

Two approaches were used to estimate the maximum rolling shear stress, $\tau_{r,max}$ at the ultimate load in the tests. First, Eq. 15 as proposed by Muster (2020) was used:

$$\tau_{\mathrm{r,max,i}} = \frac{1.5 \cdot V_{\mathrm{i}} \cdot K_{\mathrm{A}} \cdot K_{\mathrm{edge}}}{b_{\mathrm{eff,i}} \cdot t_{\mathrm{CLT}}} \qquad \text{Eq. 15}$$

Where V_i is the shear force in each direction, determined by a FE model in RFEM, using the experimentally observed punching shear resistance as input; K_A is the shear stress

distribution adjustment factor (Table 2); K_{edge} is the edge column at opening adjustment factor, computed using Eq. 17; b_{eff} is effective support width, computed using Eq. 16, as shown in Figure 5, and t_{CLT} is the thickness of the CLT.

$$b_{\mathrm{eff,i}} = b_{\mathrm{A,i}} + t_{\mathrm{CLT}} \cdot tan\,35° \quad \text{Eq. 16}$$

$$K_{\mathrm{edge}} = 1 + \frac{w_o}{3 \cdot b_{\mathrm{A,i}}} \quad \text{Eq. 17}$$

where $b_{A,i}$ is point-support dimension in each direction.

Table 2. Shear stress distribution adjustment factor (K_A).

Ratio of $b_{A,i}/t_{CLT}$	≤1	≤1.5	≤2
$K_{A,\ corner/edge\ columns}$	1.35	1.5	1.65
$K_{A,\ centre\ columns}$	1.0	1.0	1.0

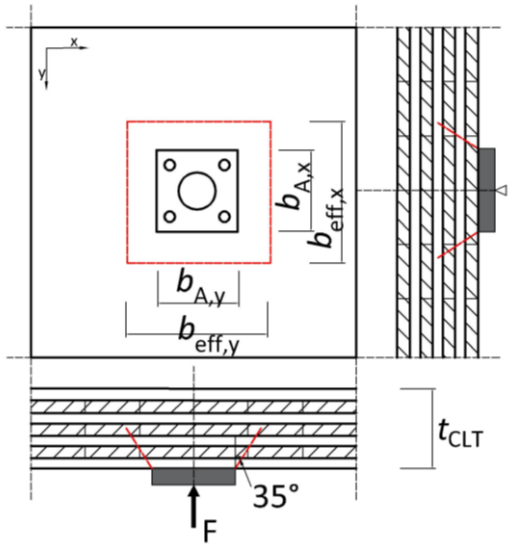

Figure 5. Geometric parameters in Muster (2020) model.

In addition, the $\tau_{r,max}$ was also calculated with the shear analogy (SA) method (Kreuzinger 1999; Mestek, 2011; Karacabeyli & Gagnon, 2019). The adjustment factor of rolling shear resistance in punching ($k_{r,pu}$) was calculated as the ratio of the maximum rolling shear stress from punching shear tests to the average of the RS strength from in-plane shear tests (Ganjali et al., 2023):

$$K_{\mathrm{r,pu}} = \frac{\tau_{\mathrm{r,max}}}{f_{\mathrm{s,mean}}} \quad \text{Eq. 18}$$

The experimental elastic support stiffness ($C_{u,z,exp}$) values were calculated as the ratio of a reference compressive stress at the load level (F) that ensured the CLT to remain in the elastic region, to support deformation using Eq. 19:

$$C_{\mathrm{u,z,exp}} = \frac{\sigma_{\perp}}{\Delta z} = \frac{F}{A_{\mathrm{net}} \cdot \Delta z} \qquad \text{Eq. 19}$$

where A_{net} is net support area and Δ_z is vertical displacement (indentation depth).

2.3 Numerical modelling

To determine the shear stresses through FE analysis (FEA), the panels were modelled as 2D plates in Dlubal's RFEM adopting RF-Laminate. The panel geometry was defined as a rectangular surface in accordance with the experimental setups. All loaded areas and the point-supports (corner series only) were modeled as separate surface elements integrated with the rest of the panel. The boundary conditions of edge, centre, and perimeter supports was modelled as roller line-supports with locked in-plane displacement in accordance with Figure 2. The supports in the corner-series, however, were modelled as surface supports (Figure 6a) having the effective bearing areas calculated with Eq. 16 and adopting a support stiffness, $C_{\mathrm{u,z}}$, of 1.7 N/mm^3, determined from the experimental results of the present study. Test loads of edge, centre, and perimeter condition series were applied on a surface equal to the effective bearing area of point supports calculated with Eq. 16 as shown in Figure 2. For the edge series, due to symmetry only a half panel was modeled (Figure 6b). The test load of the corner series was applied on a 600 mm × 600 mm surface in the centre of the panel. The material properties were assigned using RF-Laminate modules by entering the layers' thickness and their manufacturer-provided material properties. In RF-Laminate, details of composites, the option for considering coupling effect was selected for all series, and cross laminated timber without glue at narrow sides was unchecked for series S4, S5, and S6. The local X-axis was set to be parallel to the major direction of the panels. The mesh size was 30 mm with refinements around point supports.

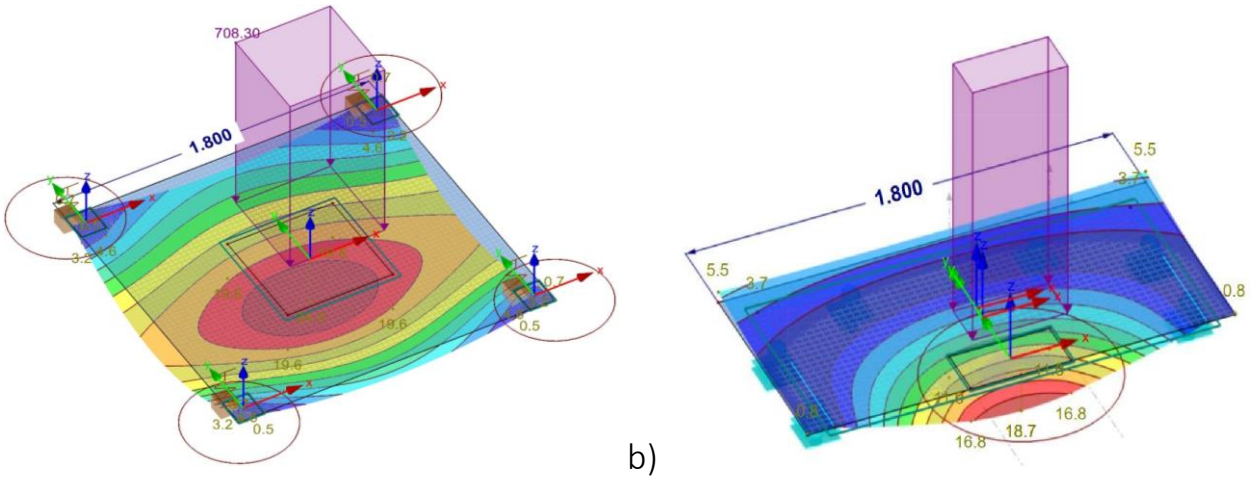

a) b)

Figure 6. RFEM model of a corner-column panel (a) and an edge-column panel (b)

3 Results and discussion

3.1 Load-displacement behaviour and failure modes

Figure 7 shows representative load-displacement curves obtained from testing. All specimens exhibited a quasi-linear behaviour up to the ultimate load. Typically, the tests were stopped after a 10% drop in the load. This was done because in a gravity load system and for the objectives of this study, observing further load drops was of no interest. However, for a few series, one specimen was pushed to the full actuator stroke to investigate the point-supported panel's ability to develop large displacement and disproportionate collapse mechanism.

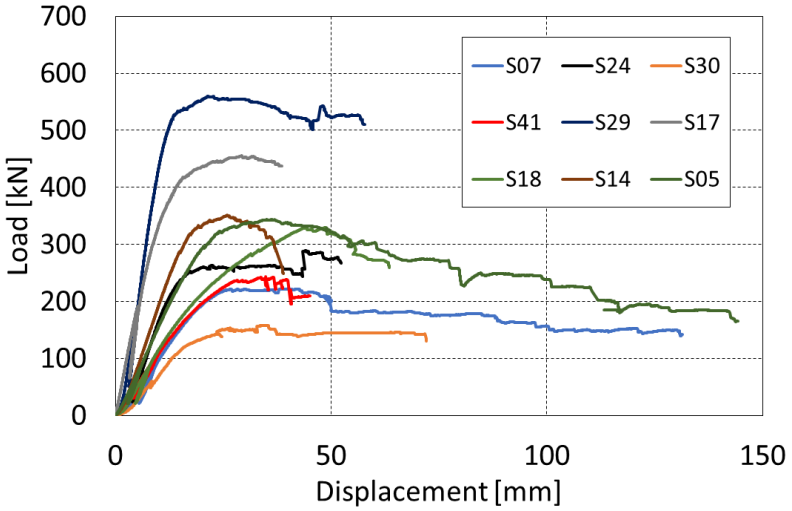

Figure 7. Representative load-displacement curves.

Local failure always initiated with minor audible rolling shear cracks (not visible), followed by rolling shear failure of lamellas near the loaded area (Figure 8a). The load was redistributed multiple times before and after the major load drop. As the displacement increased, the tension face lamellas of the panel close to the support failed in bending (Figure 8b); at larger displacements, global panel failure was observed (Figure 8c).

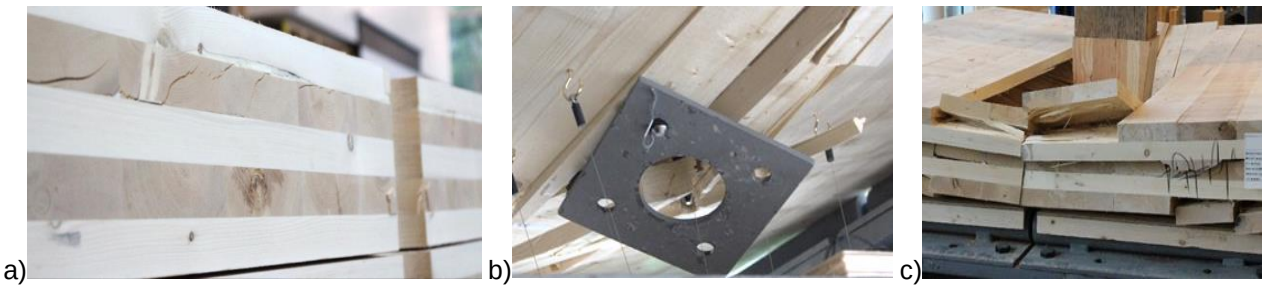

Figure 8. Failure modes under punching shear: a) rolling shear failure close to the point support; b) tensile failure of the underside boards; c) delamination at large displacement.

3.2 Punching shear resistance

The average punching shear resistance, $R_{pu,avrg.}$, of each series and the corresponding COV are summarized in Table 3. The results show CLT panels having the same CLT thickness, grade, species, and manufacturer, supported on different locations had substantially different resistances.

Table 3. Punching shear resistance obtained from testing along with the analytical and numerical maximum shear stresses.

Series	$R_{pu,avrg}$ [kN]	COV [%]	$f_{s,avrg}$ [MPa]	$\tau_{r,ult,Muster}$ [MPa]	$\tau_{r,max,FEA}$ [MPa]	$K_{r,pu,FEA}$ [-]	$K_{TW,FEA}$ [-]
S01	259.8	3.9	1.12	3.40	2.99	2.7	1.5
S02	273.9	5.5	1.48	3.59	3.12	2.1	1.5
S03	262.3	9.4	1.06	3.44	2.95	2.8	1.5
S04	321.1	2.1	1.51	4.20	3.66	2.4	1.5
S05	347.6	2.2	1.51	3.89	2.61	1.7	1.4
S06	221.2	12.3	1.14	2.89	2.54	2.2	1.5
S07	231.2	6.8	1.62	3.02	2.64	1.6	1.5
S08	322.2	3.2	1.44	4.21	3.70	2.6	1.5
S09	243.7	4.8	1.06	3.19	2.80	2.6	1.5
S10	335	3.9	1.62	3.17	2.06	1.3	1.2
S11	324	3.9	1.62	4.08	3.37	2.1	1.5
S12	259.4	5.0	1.62	[-]	2.73	1.7	[-]
S13	265.8	5.1	1.62	3.44	2.67	1.6	1.4
S14	352.5	6.3	1.62	2.74	2.27	1.4	1.3
S15	209.2	6.1	1.62	2.71	2.39	1.5	1.6
S16	259.2	3.6	1.62	3.36	2.96	1.8	1.5
S17	463.2	7.3	1.62	3.02	2.46	1.5	1.2
S23	217.8	7.5	1.62	2.82	2.48	1.5	1.5
S24	268	7.3	1.62	1.98	2.50	1.5	1.1
S25	271.5	2.4	1.62	[-]	2.75	1.7	1.1
S26	363	7.7	1.62	1.71	2.44	1.5	1.1
S27	307.4	6.6	1.62	2.27	2.78	1.7	1.1
S28	288.5	3.5	1.62	2.13	2.61	1.6	1.1
S29	566.5	3.8	1.62	2.35	2.42	1.5	1.1
S30	151.8	12.5	1.62	1.87	1.40	0.9	1.0
S30.7*	175	[-]	1.47	2.38	1.74	1.2	1.1
S30.8*	215	[-]	1.48	2.93	2.14	1.4	1.1
S41	255	5.6	1.62	2.38	4.20	2.6	1.7
S42	387.8	8.9	1.62	2.28	2.97	1.8	1.5

Figure 9a shows the effect of column location on the punching shear resistance of the series, highlighting the necessity of a proper shear stress distribution adjustment factor. The setup used for series S30 with perimeter support did not result in punching

shear failure. Therefore, two additional panels were tested with clamped ends at the line support in the minor direction; denoted with * in Table 3. That change helped activate two-way load distribution and better represent this column condition.

The impact of CLT manufacturer, grade and species is illustrated in Figure 9b. Among the 175 mm SPF edge column series, S05 (manufacturer B) had a 40% larger resistance than S07 (manufacturer F). This could be attributed to the effect of manufacturing process pressure on the RS strength as Yawalata and Lam (2011) described. Grade E1 series was 5% stronger than grade V2 series (S06 vs. S07) since punching shear failure is accompanied by the tensile failure, and E1 grade has boards with higher tensile strength in the longitudinal layers. D Fir series (S08) outperformed most SPF series; the average punching shear resistance of S08 was 40% higher when compared to the SPF series of the same manufacturer. This difference was 10% for the Hemlock series (compare S09 with S07).

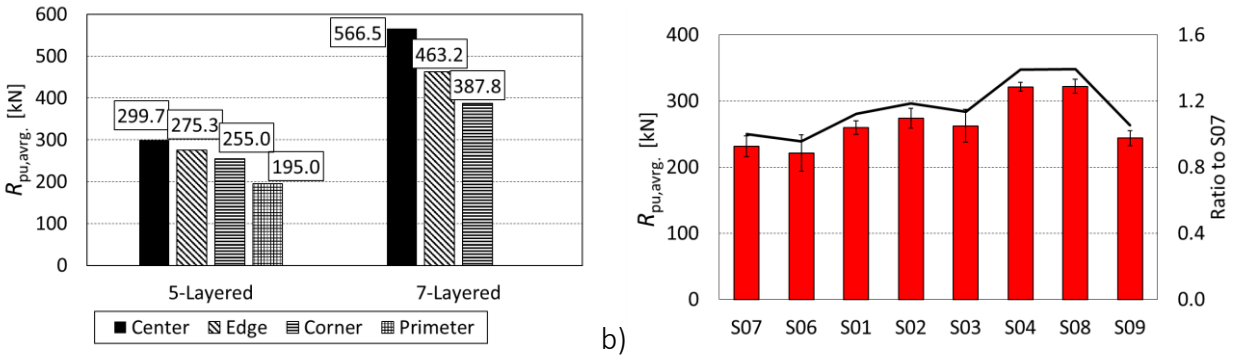

Figure 9. Impact of support condition (a); and provider, wood species, and stress grade on R_{pu} (b).

The effect of column geometry on the load-carrying capacity is shown in Figure 10. A 45% and 40% increase was attained when X- and Y-oriented rectangular columns (Figure 3c and d) were adopted. The softer (thinner) load distribution plate in S13 resulted in a 13% increase in $R_{pu,avrg}$; this can be attributed to the reduced stress concentration, Figure 10a. In the edge column series, using a round column increased the capacity by 12%. However, the results of the round column series with center column condition, S25, Figure 10b showed no increase when compared to S24 with a square load distribution plate.

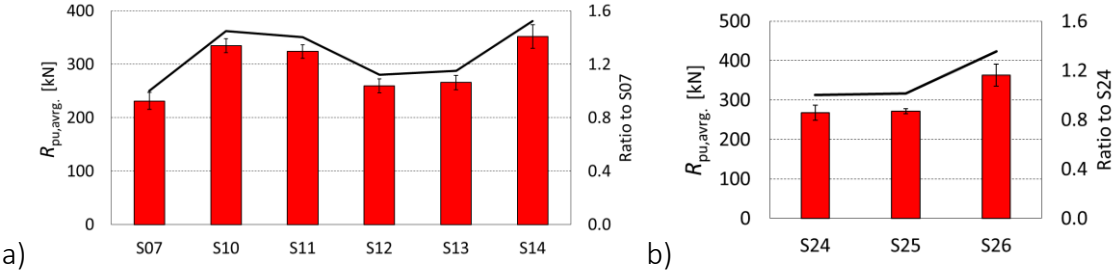

Figure 10. Column shape and size impact in edge column series (a); and centre column series (b).

Figure 11a shows that a bigger support width in the governing direction did not necessarily result in a higher capacity, but a larger support area, regardless of geometry, predicted up to 50% higher punching shear resistance (Figure 11b).

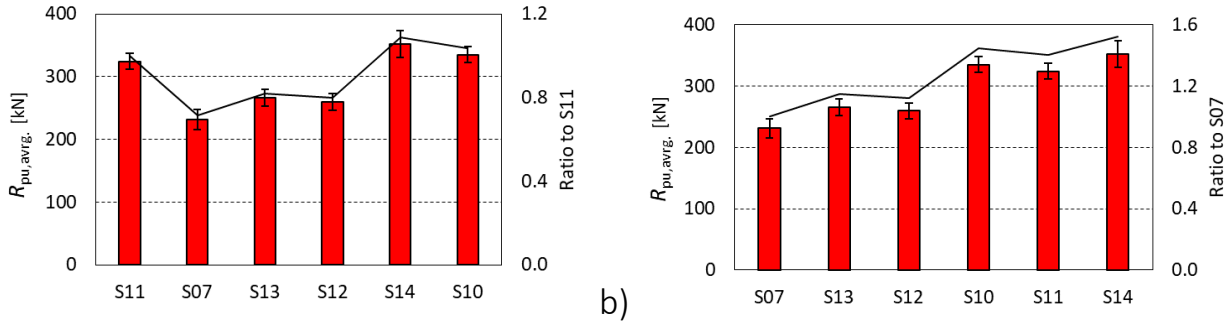

Figure 11. Impact of support width (a); and support area (b) on CLT punching shear resistance.

3.3 Magnitude and distribution of rolling shear stresses

The maximum rolling shear stress ($\tau_{S,max,Muster}$) values calculated with Muster (2020) equation, those determined through FEA ($\tau_{S,max,FEA}$), and the adjustment factor for rolling shear resistance in punching from FEA ($k_{r,pu,FEA}$) are reported in Table 3. The values of $\tau_{S,max,FEA}$ were considerably higher than those reported in Ganjali et al. (2023). The $k_{r,pu,FEA}$ values for the edge-column series averaged 2.0; for the centre column series 1.6; for the perimeter and perimeter* series 1.0 and 1.3; and for the corner series 2.2.

All shear stress distribution models discussed before give the shear stress profile across the thickness while assuming a constant profile along the width. This assumption only holds true in a one-way bending problem such as when CLT panels are supported by walls. In a point supported CLT, the two-way bending of the panel leads to a different shear stress profile along the support dimensions. Therefore, an adjustment factor for shear stress distribution in two-way bending (K_{TW}) was defined as the ratio of $\tau_{r,max,FEA}$ to $\bar{\tau}_{r,FEA}$:

$$K_{TW} = \frac{\tau_{r,max,FEA}}{\bar{\tau}_{r,FEA}} \qquad \text{Eq. 20}$$

The $K_{TW,FEA}$ of the tested series are reported in Table 3. $K_{TW,FEA}$ for the edge-column series averaged 1.5; for the centre column series averaged 1.1; for the perimeter* series averaged 1.1; and for the corner series 1.6. Using the proposed K_{TW} is contingent on the ability of adopted stress distribution model in giving the same $\bar{\tau}_r$ as those of from FEA.

The model proposed by Muster (2020) assumes a parabolic shear profile across CLT thickness and was developed for asymmetrical CLT layup meaning that it does not differentiate between the CLT thickness contributing to shear resistance in major and minor directions of a symmetric CLT layup. As shown in Table 3, This model resulted in

overestimating the $\overline{\tau}_r$ values and when its adjustment factors were applied overestimated the $\tau_{r,max}$ values, especially for the edge column series. SA method, however, accounts for the effect of transverse layers and predicted the same $\overline{\tau}_{r,max}$ values as the FE model; as an example, $\overline{\tau}_r$ through SA method and Muster (2020) in major and minor directions of S20 are compared in Figure 12a and b. Nevertheless, SA method has many steps and could make the design process laborious.

Therefore, herein, adopting the Transformed Composite Section (TCS), Figure 12e, is proposed which can be easily adopted through the following steps: 1) calculate the ratio of the longitudinal layers' modulus of elasticity (E) to the transverse layers' E; 2) determine the transformed width of the transverse layers ($b_{trans.}$) through dividing the effective width of the shear plane by the ratio calculated in step 1; 3) calculate the first moment of area of the transformed section ($Q_{trans.}$) at the desired CLT depth, excluding the outermost layers for the minor direction; 4) calculate the second moment of area of the transformed section ($I_{trans.}$), excluding the outermost layers for the minor direction; 5) calculate the rolling shear stress (τ_r) by Eq. 21:

$$\tau_r = \frac{V_i \cdot Q_{trans}}{I_{trans} \cdot b_{eff}} \qquad \text{Eq. 21}$$

Where V_i is the shear force from force analysis; Q_{trans} is the first moment of inertia of the transformed section, I_{trans} is the moment of inertia of the transformed section; and b_{eff} is the effective width of the shear plane.

The shear stress distribution of S29 in both directions through SA and TCS methods are compared in Figure 12c and d; where the simpler method, TCS, is shown to result in the same shear profile and the ultimate shear stress as SA method.

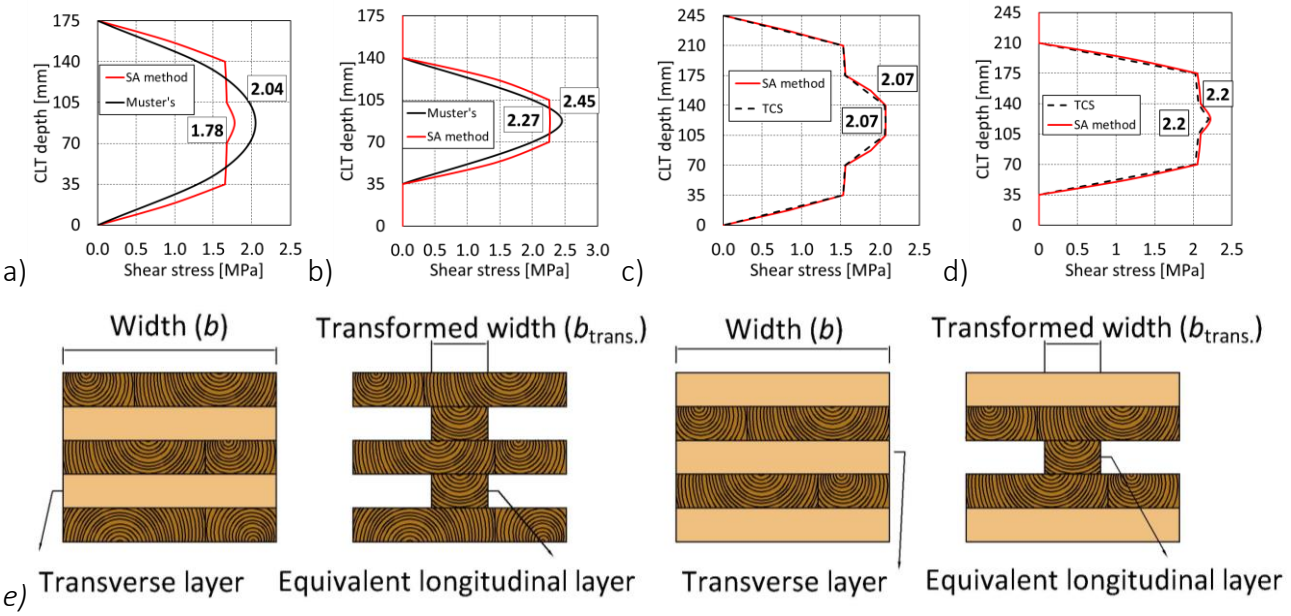

Figure 12. SA vs. Muster (2020) method in major (a) and minor (b) directions; SA vs. TCS in major (c) and minor (d) directions; TCS method description (e).

3.4 Point-support stiffness

The average $C_{u,z,exp}$ values at a reference compressive stress level of 3.6 MPa are compared with those proposed by Muster (2020) in Table 4. The average $C_{u,z,exp}$ for 175 mm thick and 245 mm thick panels were 1.69 N/mm^3 and 1.73 N/mm^3 respectively. These experimentally determined values do not confirm Muster (2020) values for different CLT thicknesses. The performed one-way ANOVA test with a P-value of 0.78 showed no statistically significant difference between the $C_{u,z,exp}$ of 5- and 7-layered panels, suggesting on average a $C_{u,z}$ of 1.71 N/mm^3 for SPF CLT panels having E1 stress grade regardless of thickness. The experimentally determined $C_{u,z}$ in this study can be adopted for a FEA based design of point supported CLT floors.

Table 4. Elastic support stiffness values.

CLT thickness [mm]	$C_{u,z,Muster}$ [N/mm^3]	$C_{u,z,exp}$ [N/mm^3]	Specimen count	COV [%]
175	0.3	1.69	30	24
245	0.86	1.73	24	31

3.5 Proposed analytical model

For punching shear design of point supported CLT, the simple yet accurate TCS stress distribution model is used along with the required material-strength related, and column-condition related adjustment factors. The TCS method results in the same shear stress profile as the SA method but is easier to implement. The experimentally determined punching shear adjustment factor, $k_{r,pu}$, for the rolling shear resistance for different column conditions (Table 5) are higher than the $k_{r,pu}$ of 1.6 recommended in prEN1995 (2023) for all column conditions, except for perimeter column condition. therefore, prEN1995 (2023) seems overly conservative for centre, edge, and corner columns. The proposed adjustment factor for shear stress distribution in two-way bending (K_{TW}) for different column conditions can be adopted for both TCS and SA methods resulting in the same maximum rolling shear stress from 2D FEA in RFEM. Thus, when designing point supported CLT, Eq. 22 should be satisfied:

$$\tau_{r,d} \geq \tau_{r,max} \qquad \text{Eq. 22}$$

$$\tau_{r,d} = K_{r,pu} \cdot f_s \qquad \text{Eq. 23}$$

Where $\tau_{r,d}$ is the design rolling shear stress; f_s is rolling shear strength of CLT; and $k_{r,pu}$ is based on Table 5.

Table 5. Rolling shear resistance in punching shear adjustment factor ($k_{r,pu}$).

Column location	Centre	Edge	Corner	Perimeter
$k_{r,pu}$	1.6	2	2.2	1.3

The maximum rolling shear stress ($\tau_{r,max}$) in the decisive layer can be calculated by:

$$\tau_{\mathrm{r,max}} = \frac{V_{\mathrm{i}} \cdot Q_{\mathrm{trans}} \cdot K_{\mathrm{TW}}}{I_{\mathrm{trans}} \cdot b_{\mathrm{eff}}} \qquad \text{Eq. 24}$$

Where $b_{eff,i}$ is determined with Eq. 25 and Eq. 26 according to Figure 13 for the cases where the panel is continuous on the both sides of the point support and when it is not, respectively; and K_{TW} is based on Table 6.

$$b_{\mathrm{eff},1} = b_{\mathrm{A,i}} + t_{\mathrm{CLT}} \cdot tan\,35° \qquad \text{Eq. 25}$$

$$b_{\mathrm{eff},2} = b_{\mathrm{A,i}} + 0.5 \cdot t_{\mathrm{CLT}} \cdot tan\,35° \qquad \text{Eq. 26}$$

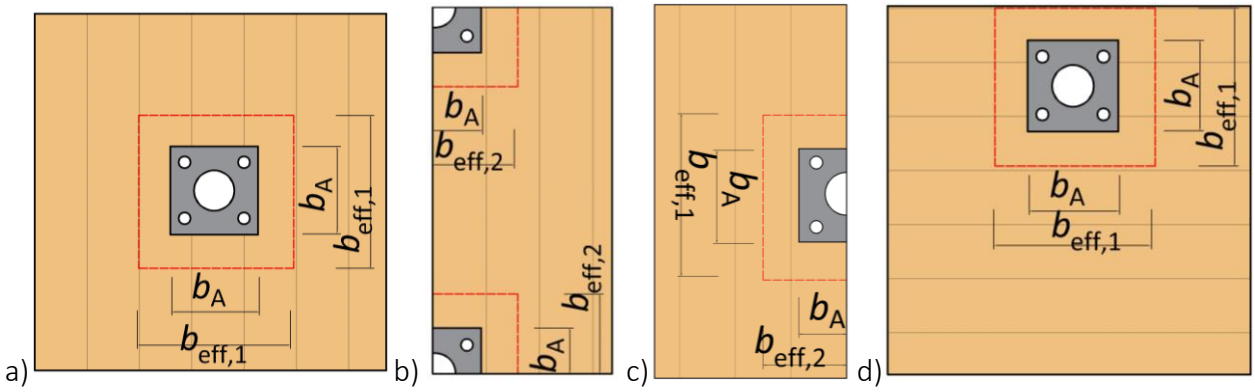

Figure 13. Determination of b_{eff} in centre (a); corner (b); edge (c); and perimeter (d) columns.

Table 6. Adjustment factor for shear stress distribution in two-way bending (K_{TW}).

Column type	Centre	Edge	Corner	Perimeter
K_{TW}	1.1	1.5	1.6	1.1

4 Conclusions and outlook

Based on the punching shear tests on 164 full-scale CLT panels, and subsequent analytical and numerical analyses, the following conclusions can be drawn:

- Column location impacted the punching shear resistance, R_{pu}, highlighting the need for incorporating a shear stress distribution adjustment factor in CLT punching shear design.
- Douglas Fir and Hemlock series were 40% and 10% stronger than SPF panels from the same provider, respectively. Panels from different manufacturers with the same grade and species were up to 40% stronger.
- A larger support area (regardless of geometry) and softer (thinner) load distribution plate increased the resistance by 50% and 13%, respectively. Overall, the E1 series were slightly (5%) stronger than V2 series.

- Round column geometry increased the resistance of the edge column panels while it had no effect on the punching shear resistance $R_{pu,avrg}$ of the centre column series.
- The adjustment factor for rolling shear resistance in punching shear, $k_{r,pu,FEA}$, for the edge-column series averaged at 2.0; for the centre column series it averaged at 1.6; for the perimeter and perimeter* series averaged at 1.0 and 1.3; for the corner series it was 2.2 and in total averaged at 1.8.
- An adjustment factor for shear stress distribution in two-way bending (K_{TW}) was introduced. Based on the tests, K_{TW} should be 1.5 for the edge-column series; 1.1 for the centre column series; 1.1 for the perimeter* series; and 1.6 for the corner series.
- Simple beam bending model overestimated the shear stresses in CLT, whereas adopting the SA method resulted in more accurate shear stress profile across CLT thickness. To avoid the laborious SA method, the TCS method is proposed that leads to the same shear stress profile as the SA method.
- The average experimentally determined elastic support stiffness, $C_{u,z,exp}$, for 175 mm thick and 245 mm thick CLT panels were 1.69 N/mm^3 and 1.73 N/mm^3; this does not confirm Muster (2020) equation values.
- A model for punching shear design of CLT based on TCS method is proposed with the required adjustment factors accounting for the effect of concurrent RS and compression perpendicular stresses as well as the effect of two-way bending on the maximum RS shear.
- Even with the proposed analytical model and the required support-condition and material-strength related adjustment factors, point supported CLT design requires a FE force-analysis. Therefore, a simple force analysis method will be developed in the next phase of this project.

Acknowledgments

The project was supported by the Province of British Columbia's 'Green Construction Through Wood' program and the Natural Sciences and Engineering Research Council of Canada through an Alliance grant. The support by the UNBC laboratory technicians James Andal, Nathan Downie, and Ryan Stern, as well as Fast + Epp Concept Lab manager Brandon Sullivan and Concept Lab technician Bernhard Zarnitz is appreciated.

References

Bogensperger T, Jöbstl R A (2015) Concentrated Load Introduction in CLT Elements perpendicular to Plane. In proc. INTER, Šibenik, Croatia.

CSA-O86 (2024) Engineering Design in Wood. Canadian Standards Association, Mississauga, Canada.

Dunham, C W (1944) The theory and practice of reinforced concrete, 2nd edition McGraw-Hill Book Co., Inc, New York, USA.

Ganjali, H et al. (2023) Punching-shear strength of point-supported CLT floor panels. In proc. INTER, Biel, Switzerland.

ISO 6891 (1983) Timber structures, Joints made with mechanical fasteners, General principles for the determination of strength and deformation characteristics, International Organization for Standardization (ISO).

Karacabeyli, E, & Gagnon, S (2019) Canadian CLT Handbook, 2019 Edition. FPInnovations, Canada.

Kreuzinger, H (1999) Platten, Scheiben und Schalen–ein Berechnungsmodell für gängige static program. Bauen Mit Holz 1: 34–39.

Mestek, P & Dietsch, P (2013) Design concept for CLT-reinforced with self-tapping screws. In Focus Solid Timber Solutions-European Conference on Cross Laminated Timber (CLT). Graz, Austria

Mestek, P (2011) Punktgestützte Flächentragwerke aus Brettsperrholz – Schubbemessung unter Berücksichtigung von Schubverstärkungen (in German). Technical University, Munich (Doctoral Thesis).

Muster, M (2020) Column-Slab Connection in Timber Flat Slabs. ETH, Zurich (Doctoral Thesis).

NDS (2024) National Design Specification for Wood Construction. American Wood Council.

Popovski, M et al. (2016) Structural behaviour of Point-supported CLT floor Systems. In proc. WCTE. Vienna, Austria

prEN 1995-1-1 (2023) Eurocode 5 for CEN enquiry - Design of timber structures - part 1-1: General rules and rules for buildings. European Committee for Standardization, Brussels, Belgium.

Slotboom, C et al. (2023) A Comparison of Punching Shear Design Approaches for Point Supported CLT Panels. In proc. WCTE.

Yawalata D, Lam F (2011) Development of technology for cross laminated timber building systems. Research report submitted to Forestry Innovation Investment Ltd. Vancouver, BC, Canada: University of British Columbia.